JOURNAL OF MULTIFUNCTIONAL MATERIALS & PHOTOSCIENCE
10(2), December 2019, pp. 105-112

Synthesis of LiLa(MoO4)2:Eu^{3+}/Yb^{3+} Phosphors via Microwave-Assisted Sol- Gel Route and Their Spectroscopic Properties

Won-Chun Oh, Ji Soon Park, Eung Gyun Kim, Hak Su Kim, Chang Sung Lim*

Department of Aerospace Advanced Materials & Chemical Engineering, Hanseo University, *Korea*

Abstract: LiLa1-x(MoO4)2:Eu3+/Yb3 phosphors with doping concentrations of Eu3+ and Yb3+ (x = Eu3+ + Yb3+, Eu3+ = 0.05, 0.1, 0.2 and Yb3+= 0.2, 0.45) were successfully synthesized by the microwave-assisted sol-gel process, and their structural and spectroscopic properties were investigated. Well-crystallized particles showed a fine and homogeneous morphology with particle sizes of 5-10 μm. Under excitation at 980 nm, LiLa0.5(MoO4)2:Er0.05Yb0.45 particles exhibited a weak 475-nm emission band in the blue region, a strong 525-nm and a weak 550-nm emission bands and in the green region, and a very weak 655-nm emission band in the red region. The spectroscopic features of Raman spectra were discussed in terms of the superposition of Eu3+ luminescence and vibrational lines. The possibility of controlling the spectral distribution of upconversion luminescence by the chemical content of molybdate hosts is demonstrated.

Keywords: LiLa(MoO4)2:Eu3+/Yb3+, Phosphors, Microwave-assisted, Spectroscopic properties.

Introduction

Photoluminescence particles have evolved in their applications, such as fluorescent lamps, cathode ray tubes, solid-state laser, amplifiers for fiber optics communication and new optoelectronic devices, which show high luminescence quantum yields, since usually more than one metastable excited state exists, multiple emissions are observed [1, 2]. Rare earth activated upconversion (UC) particles can convert near infrared radiation of low energy into visible radiation of high energy. Recently, the synthesis and the luminescence properties of UC particles have attracted considerable interest since they are considered as potentially active components in new optoelectronic devices and luminescent labels for imaging and biodetection assays, which overcome the current limitations in traditional photoluminescence materials [3]. It is possible for the trivalent rare earth ions in the disordered tetragonal-phase to be partially substituted by Eu^{3+} and Yb^{3+} ions, these ions are effectively doped into the crystal lattices of the tetragonal phase due to the similar radii of the trivalent rare earth ions in R^{3+}, this results in the excellent

* Corresponding author: *cslim@hanseo.ac.kr*

UC photoluminescence properties [4-6]. Among rare earth ions, the Eu^{3+} ion is suitable for converting infrared to visible light through the UC process due to its appropriate electronic energy level configuration. The co-doped Yb^{3+} ion and Eu^{3+} ion can remarkably enhance the UC efficiency for the shift from infrared to visible light due to the efficiency of the energy transfer from Yb^{3+} to Eu^{3+}. The Yb^{3+} ion, as a sensitizer, can be effectively excited by an incident light source energy. This energy is transferred to the activator from which radiation can be emitted. The Eu^{3+} ion activator is the luminescence center of the UC particles, while the sensitizer enhances the UC luminescence efficiency [7-9].

Recently, rare earth activated molybdate compounds have attracted great attention UC photoluminescence properties. To have a possibility for an optimal material selection in laser and photonic fields, it is required to design and synthesize new complex tmolybdate compounds with stable crystal structures and excellent UC luminescent properties. Several processes have been developed to prepare these rare-earth-doped double molybdates [10-17], Usually, double molybdates are prepared by a solid-state method that requires high temperatures, a lengthy heating process and subsequent grinding, these results in a loss of the emission intensity and an increase in cost. The sol-gel process provides some advantages over the conventional solid-state method, including good homogeneity, low calcination temperature, small particle size and narrow particle size distribution optimal for good luminescent characteristics. However, the sol-gel process has a disadvantage in that it takes a long time for gelation. Compared with the usual methods, microwave-assisted sol-gel synthesis has the advantages of a very short reaction time, small-size particles, narrow particle size distribution, and high purity of final polycrystalline samples. Microwave heating is delivered to the material surface by radiant and/or convection heating, which is transferred to the bulk of the material via conduction [18, 19].

In this study, $LiLa_{1-x}(MoO_4)_2:Eu^{3+}/Yb^{3+}$ phosphors with doping concentrations of Eu^{3+} and Yb^{3+} ($x = Eu^{3+} + Yb^{3+}$, $Eu^{3+} = 0.05, 0.1, 0.2$ and $Yb^{3+} = 0.2, 0.45$) phosphors were prepared by the microwave-assisted sol-gel process followed by heat treatment. The synthesized particles were characterized by X-ray diffraction (XRD), scanning electron microscopy (SEM), and energy-dispersive X-ray spectroscopy (EDS). The optical properties were examined comparatively using photoluminescence (PL) emission and Raman spectroscopy.

Experimental

Appropriate stoichiometric amounts of $HLiO \cdot H_2O$ (99 %, Sigma-Aldrich, USA), $La(NO_3)_3 \cdot 6H_2O$ (99 %, Sigma-Aldrich, USA), $(NH_4)_6Mo_7O_{24} \cdot 4H_2O$ (99%, Alfa Aesar, USA), $Eu(NO_3)_3 \cdot 5H_2O$ (99.9%, Sigma-Aldrich, USA), $Yb(NO_3)_3 \cdot 5H_2O$ (99.9%, Sigma-Aldrich, USA), citric acid (99.5%, Daejung Chemicals, Korea), NH_4OH (A.R.), ethylene glycol (A.R.) and distilled water were used to prepare $LiLa(MoO_4)_2$, $LiLa_{0.8}(MoO_4)_2:Eu_{0.2}$, $LiLa_{0.7}(MoO_4)_2:Eu_{0.1}Yb_{0.2}$ and $LiLa_{0.5}(MoO_4)_2:Eu_{0.05}Yb_{0.45}$ compounds with doping concentrations of Eu^{3+} and Yb^{3+} ($Eu^{3+} = 0.05, 0.1, 0.2$ and $Yb^{3+} = 0.2, 0.45$). To prepare $LiLa(MoO_4)_2$, 0.4 mol% $HLiO \cdot H_2O$ and 0.114 mol% $(NH_4)_6Mo_7O_{24} \cdot 4H_2O$ were dissolved

in 20 mL of ethylene glycol and 80 mL of 5M NH_4OH under vigorous stirring and heating. Subsequently, 0.4 mol% $La(NO_3)_3 \cdot 6H_2O$ and citric acid (with a molar ratio of citric acid to total metal ions of 2:1) were dissolved in 100 mL of distilled water under vigorous stirring and heating. Then, the solutions were mixed together under vigorous stirring and heating at 80-100°C. At the end, highly transparent solutions were obtained and adjusted to pH=7-8 by the addition of 8M NH_4OH. In order to prepare $LiLa_{0.8}(MoO_4)_2:Eu_{0.2}$, the mixture of 0.32 mol% $La(NO_3)_3 \cdot 6H_2O$ with 0.08 mol% $Eu(NO_3)_3 \cdot 5H_2O$ was used for the creation of the rare earth solution. In order to prepare $LiLa_{0.7}(MoO_4)_2:Eu_{0.1}Yb_{0.2}$, the mixture of 0.28 mol% $La(NO_3)_3 \cdot 6H_2O$ with 0.04 mol% $Eu(NO_3)_3 \cdot 5H_2O$ and 0.08 mol% $Yb(NO_3)_3 \cdot 5H_2O$ was used for the creation of the rare earth solution. In order to prepare $LiLa_{0.5}(MoO_4)_2:Eu_{0.05}Yb_{0.45}$, the rare earth containing solution was generated using 0.2 mol% $La(NO_3)_3$′″$6H_2O$ with 0.02 mol% $Eu(NO_3)_3 \cdot 5H_2O$ and 0.18 mol% $Yb(NO_3)_3$′″$5H_2O$. The chemical compositions of the sample notations are given in Table 1.

Table 1

Chemical composition: / Sample notation:	HLiO-H_2O (mol%)	$(NH_4)_6Mo_7O_{24}$·$4H_2O$ (mol%)	$La(NO_3)_3$·$6H_2O$ (mol%)	$EuNO_3$·5H2O (mol%)	$Yb(NO_3)_3$·$5H_2O$ (mol%)
(a) $LiLa_3(MoO_4)_2$	0.4	0.114	0.4		
(b) $LiLa_{0.8}(MoO_4)_2:Eu_{0.2}$	0.4	0.114	0.32	0.08	
(c) $LiLa_{0.7}(MoO_4)_2:Eu_{0.1}/Yb_{0.2}$	0.4	0.114	0.28	0.04	0.08
(d) $LiLa_{0.5}(MoO_4)_2:Eu_{0.05}/Yb_{0.45}$	0.4	0.114	0.2	0.02	0.18

The transparent solutions were placed into a microwave oven operating at a frequency of 2.45 GHz with a maximum output-power of 1250 W for 30 min. The working cycle of the microwave reaction was controlled very precisely using a regime of 40 s on and 20 s off for 15 min, followed by further treatment of 30 s on and 30 s off for 15 min. The ethylene glycol was evaporated slowly at its boiling point. Ethylene glycol is a polar solvent at its boiling point of 197°C, this solvent is a good candidate for the microwave process. If ethylene glycol is used as the solvent, the reactions proceed at the boiling point temperature. When microwave radiation is supplied to the ethylene-glycol-based solution, the components dissolved in the ethylene glycol can couple. The charged particles vibrate in the electric field interdependently when a large amount of microwave radiation is supplied to the ethylene glycol. The samples were treated with ultrasonic radiation for 10 min to produce a light yellow transparent sol. After this, the light yellow transparent sols were dried at 120°C in a dry oven to obtain black dried gels. The black dried gels were grinded and heat-treated at 900°C for 16 h with 100°C

intervals between 600-900°C. Finally, white particles were obtained for $LiLa(MoO_4)_2$ and pink particles for the doped compositions.

The phase composition of the synthesized particles was identified using XRD (D/MAX 2200, Rigaku, Japan). The microstructure and surface morphology of the $LiLa(MoO_4)_2$, $LiLa_{0.8}(MoO_4)_2:Eu_{0.2}$, $LiLa_{0.7}(MoO_4)_2:Eu_{0.1}Yb_{0.2}$ and $LiLa_{0.5}(MoO_4)_2:Eu_{0.05}Yb_{0.45}$ particles were observed using SEM/EDS (JSM-5600, JEOL, Japan). The PL spectra were recorded using a spectrophotometer (Perkin Elmer LS55, UK) at room temperature. Raman spectroscopy measurements were performed using a LabRam Aramis (Horiba Jobin-Yvon, France). The 514.5-nm line of an Ar ion laser was used as the excitation source, and the power on the samples was kept at 0.5 mW.

Results and Discussion

Fig. 2 shows the XRD patterns of the (a) JCPDS 18-0734 data of $LiLa(MoO_4)_2$, the synthesized (b) $LiLa(MoO_4)_2$, (c) $LiLa_{0.8}(MoO_4)_2:Eu_{0.2}$, (d) $LiLa_{0.7}(MoO_4)_2:Eu_{0.1}Yb_{0.2}$ and (e) $LiLa_{0.5}(MoO_4)_2:Eu_{0.05}Yb_{0.45}$ particles. The crystal structures of (b) $LiLa(MoO_4)_2$, (c) $LiLa_{0.8}(MoO_4)_2:Eu_{0.2}$, (d) $LiLa_{0.7}(MoO_4)_2:Eu_{0.1}Yb_{0.2}$ and (e) $LiLa_{0.5}(MoO_4)_2:Eu_{0.05}Yb_{0.45}$ particles were assigned to the crystallographic data of (a) $LiLa(MoO_4)_2$ (JCPDS 18-0734). However, with increasing of the Yb^{+3} ions, the crystal structures of (c) $LiLa_{0.8}(MoO_4)_2:Eu_{0.2}$, (d) $LiLa_{0.7}(MoO_4)_2:Eu_{0.1}Yb_{0.2}$ and (e) $LiLa_{0.5}(MoO_4)_2:Eu_{0.05}Yb_{0.45}$ showed impurity phases detected at 32°, 34°, 35°, 48°and 49°. The foreign reflexes are marked with asterisk in Fig. 1(c), (d) and (e). It is assumed that these foreign reflexes are induced by the incorporation of the Eu^{3+} ions and Yb^{3+} ions for the La^{3+} ions into the $LiLa(MoO_4)_2$ crystal structure and result in the unit cell shrinkage and a new phase formation of the $[MoO_4]^{2-}$ groups.

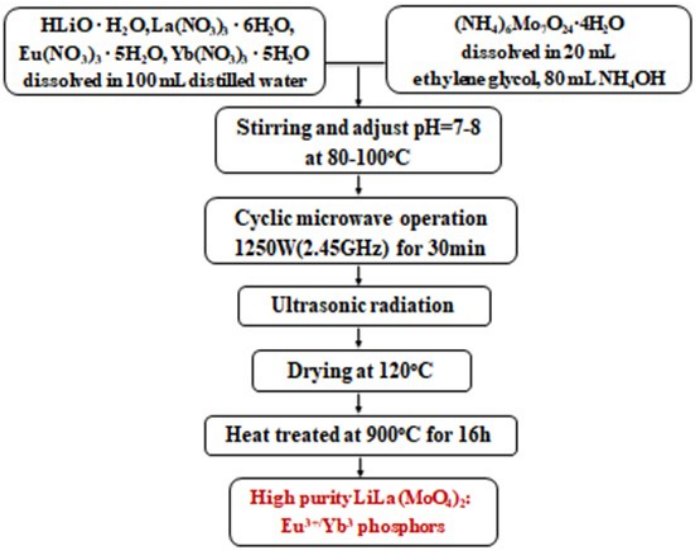

Figure 1

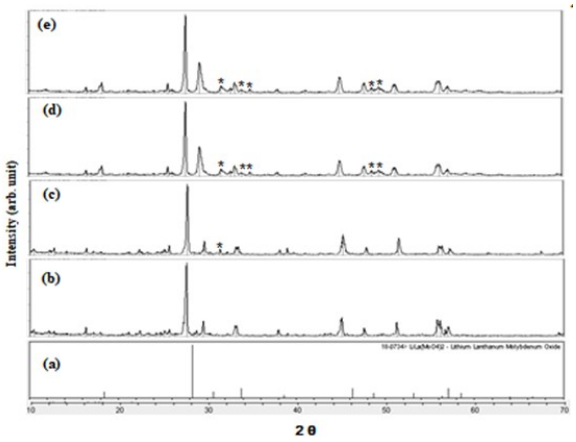

Figure 2

Fig. 3 shows a SEM image of the synthesized $LiLa_{0.5}(MoO_4)_2:Eu_{0.05}Yb_{0.45}$ particles. The as-synthesized samples are well crystallized with a fine and homogeneous morphology and particle size of 5-10 ìm. It is noted that the obtained sample possesses a partial substitution of La^{3+} by Eu^{3+} and Yb^{3+} ions, and the ions are effectively doped into crystal lattices of the $LiLa(MoO_4)_2$ phase due to the similar radii of La^{3+} and by Eu^{3+} and Yb^{3+}. This suggests that the microwave-assisted sol-gel process is suitable for the growth of $LiLa_{1-x}(MoO_4)_2:Eu^{3+}/Yb^{3+}$ crystallites.

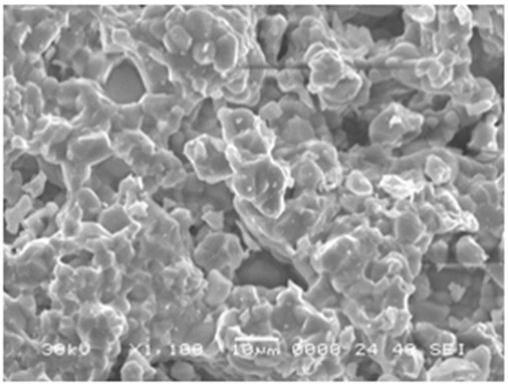

Figure 3

Fig. 4 shows the UC photoluminescence emission spectra of the as-prepared (a) $LiLa(MoO_4)_2$, (b) $LiLa_{0.8}(MoO_4)_2:Eu_{0.2}$, (c) $LiLa_{0.7}(MoO_4)_2:Eu_{0.1}Yb_{0.2}$ and (d) $LiLa_{0.5}(MoO_4)_2:Eu_{0.05}Yb_{0.45}$ particles excited under 980 nm at room temperature. The UC intensities of (d) $LiLa_{0.5}(MoO_4)_2:Eu_{0.05}Yb_{0.45}$ particles exhibited a weak 475-nm emission band in the blue region, a strong 525-nm and a weak 550-nm emission bands and in the green region, and a very weak 655-nm emission band in the red region. The weak 475-nm emission in the blue region corresponds to the $^7F_0 \rightarrow {}^5D_2$ transition. The strong 525-nm emission and the weak 550-nm in the green region correspond to the $^7F_1 \rightarrow {}^5D_1$ transition and $^5D_1$ '! ^7F_J transition, respectively. The very weak emission 655-nm band in the red region corresponds to the $^5D_0 \rightarrow {}^7F_3$ transition. The UC intensities of (a) $LiLa(MoO_4)_2$ and

(b) $LiLa_{0.8}(MoO_4)_2:Eu_{0.2}$ were not detected. The UC intensity of (d) $LiLa_{0.5}(MoO_4)_2:Eu_{0.05}Yb_{0.45}$ is much higher than that of (c) $LiLa_{0.7}(MoO_4)_2:Eu_{0.1}Yb_{0.2}$ particles. The doping amounts of Eu^{3+}/Yb^{3+} had a great effect on the morphological features of the particles and their UC fluorescence intensity. The Yb^{3+} ion sensitizer can be effectively excited by the energy of an incident light source, this energy is transferred to the activator where radiation can be emitted. The Eu^{3+} ion activator is the luminescence center for these UC particles, and the sensitizer enhances the UC luminescence efficiency [20-22].

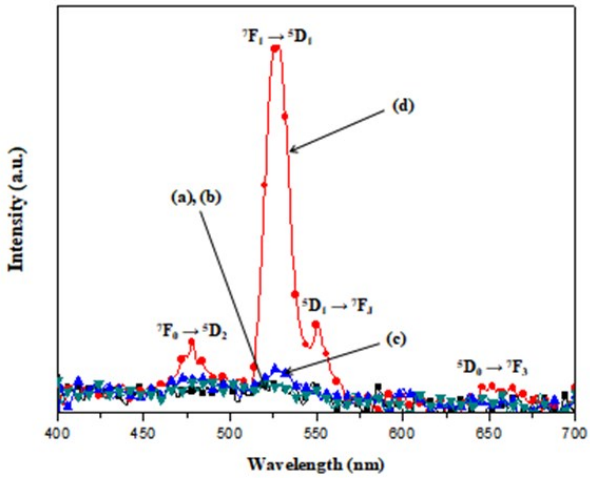

Figure 4

Fig. 5 shows the Raman spectra of the synthesized Raman spectra of the synthesized (a) $LiLa(MoO_4)_2$(LiLM), (b) $LiLa_{0.5}(MoO_4)_2:Eu_{0.05}Yb_{0.45}$(LiLM:Eu), (c) $LiLa_{0.7}(MoO_4)_2:Eu_{0.1}Yb_{0.2}$(LiLM:EuYb) and (d) $LiLa_{0.5}(MoO_4)_2:Eu_{0.05}Yb_{0.45}$(LiLM:EuYb#) particles excited by the 514.5-nm line of an Ar ion laser at 0.5 mW. The internal modes for the (a) $LiLa(MoO_4)_2$(LiLM) particles were detected at 294, 315, 330, 376, 666, 752, 818, 898 and 994cm^{-1}, respectively. The well-resolved sharp peaks for the $LiLa(MoO_4)_2$(LiLM) particles indicate a high crystallinity state of the synthesized particles. The internal vibration mode frequencies are dependent on the lattice parameters and the degree of the partially covalent bond between the cation and molecular ionic group $[MoO_4]^{2-}$. The Raman spectra of $LiLa_{0.8}(MoO_4)_2:Eu_{0.2}$, $LiLa_{0.7}(MoO_4)_2:Eu_{0.1}Yb_{0.2}$ and $LiLa_{0.5}(MoO_4)_2:Eu_{0.05}Yb_{0.45}$ particles indicated the distorted peaks at higher frequencies (664, 818, 871 and 996 cm^{-1}) and at lower frequencies (294, 315, 330 and 376 cm^{-1}). The Raman spectra of (b) $LiLa_{0.5}(MoO_4)_2:Eu_{0.05}Yb_{0.45}$(LiLM:Eu), (c) $LiLa_{0.7}(MoO_4)_2:Eu_{0.1}Yb_{0.2}$(LiLM:EuYb) and (d) $LiLa_{0.5}(MoO_4)_2:Eu_{0.05}Yb_{0.45}$(LiLM:EuYb#) particles prove that the doping ions can influence the structure of the host materials. The combination of a heavy metal cation and the inter-ionic distance for Eu^{3+} and Yb^{3+} substitutions in La^{3+} sites in the lattice result in a high probability of UC and phonon-splitting relaxation in $LiLa_{1-x}(MoO_4)_2:Eu^{3+}/Yb^{3+}$ crystals. It is assumed that these strongly dominant Raman spectra were attributed to the concentration quenching effect of Eu^{3+} ions and to the superimposition by intense Eu^{3+} luminescence lines showing drastically longer wavelengths [22].

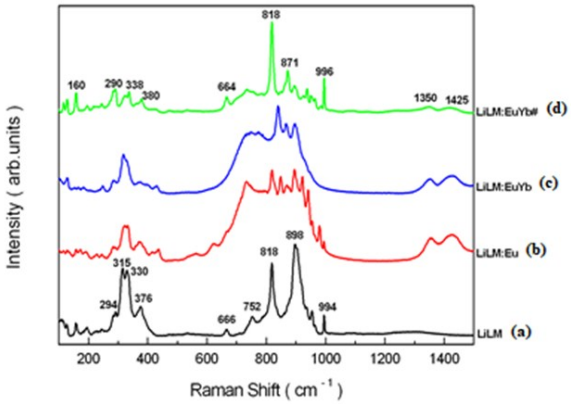

Figure 5

Conclusions

$LiLa_{1-x}(MoO_4)_2:Eu^{3+}/Yb^3$ phosphors with doping concentrations of Eu^{3+} and Yb^{3+} (x = Eu^{3+} + Yb^{3+}, Er^{3+} = 0.05, 0.1, 0.2 and Yb^{3+}= 0.2, 0.45) were successfully synthesized by the cyclic microwave-assisted sol-gel process showing a fine and homogeneous morphology with particle sizes of 5-10 ìm. The UC intensities of (d) $LiLa_{0.5}(MoO_4)_2:Eu_{0.05}Yb_{0.45}$ particles exhibited a strong 525-nm emission band in the green region, a weak 475-nm emission band in the blue region, and a very weak 655-nm emission band in the red region. The weak 475-nm emission in the blue region corresponds to the $^7F_0$ '! $^5D_2$ transition. The strong 525-nm emission and the weak 550-nm in the green region correspond to the $^7F_1$ '! $^5D_1$ transition and $^5D_1$ '! ^7F_J transition, respectively. The very weak emission 655-nm band in the red region corresponds to the $^5D_0$ '! $^7F_3$ transition. The UC intensity of $LiLa_{0.5}(MoO_4)_2:Eu_{0.05}Yb_{0.45}$ is much higher than that of $LiLa_{0.7}(MoO_4)_2:Eu_{0.1}Yb_{0.2}$ particles. The strongly dominant Raman spectra were attributed to the concentration quenching effect of Eu^{3+} ions and to the superimposition by intense Eu^{3+} luminescence lines showing drastically longer wavelengths.

Acknowledgment

This research was supported by the Basic Science Research Program through the National Research Foundation of Korea (NRF) funded by the Ministry of Science, ICT and future Planning (2018R1D1A1A09082321).

References

1 M. Lin, Y. Zho, S. Wang, M, Liu, Z. Duan, Y. Chen, F. Li, F. Xu, T. Lu, *Bio. Adv.*, 30, 1551 (2012) .

2 M.Wang, G. Abbineni, A. Clevenger, C. Mao, S. Xu, *Nanomedicine: Nanotech. Biology, and Medicine*, 7, 710 (2011).

3 A. Shalav, B.S. Richards, M.A. Green, *Sol. Ener. Mat. Sol. Cells*, 91, 829 (2007).

4 C. Guo, H. K. Yang, J.H. Jeong, *J. Lum.*, 130, 1390 (2010).

5 J. Liao, D. Zhou, B. Yang, R. liu, Q. Zhang, Q. Zhou, *J. Lum.*, 134, 533 (2013).

6 J. Sun, J. Xian, H. Du, *J. Phys. Chem. Solids*, 72, 207 (2011).

7 T. Li, C. Guo, Y. Wu, L. Li, J.H. Jeong, *J. Alloys Comps*., 540, 107 (2012).

8 M. Nazarov, D.Y. Noh, *J. Rare Earths*, 28, 1 (2010).

9 J. Sun, W. Zhang, W. Zhang, H. Du, *Mat. Res. Bull*., 47, 786 (2012).

10 H. Du, Y. Lan, Z. Xia, J. Sun, *Mat. Res. Bull*., 44, 1660 (2009).

11 M. Haque, D.K. Kim, *Mat. Lett*., 63, 793 (2009).

12 L. Qin, Y. Huang, T, Tsuboi, H.J. Seo, *Mat. Res. Bull*., 47, 4498 (2012).

13 Y. Tian, B. Chen, B. Tian, R. Hua, J. Sun, L. Cheng, H. Zhong, X. Li, J. Zhang, Y. Zheng, T. Yu, L. Huang, Q. Meng, *J. Alloy Comps*., 509, 6096 (2011).

14 Y. Tian, B. Chen, B. Tian, J. Sun, X. Li, J. Zhang, L. Cheng, H. Zhong, H. Zhong, Q. Meng, R. Hua, *Physica B*, 407, 2556 (2012).

15 Q. Chen, L. Qin, Z. Feng, R. Ge, X. Zhao, H. Xu, *J. Rare Earths*, 29, 843 (2011).

16 J. Zhang, X. Wang, X, Zhang, X. Zhao, X. Liu, L. *Peng, Inog. Chem. Comm*., 14, 1723 (2011).

17 W. Lu, L. Cheng, J. Sun, H. Zhong, X. Li, Y. Tian, J. Wan, Y. Zheng, L. Huang, T. Yu, H.Yu, B. Chen, *Physica B*, 405, 3284 (2010).

18 C.S. Lim, Infr. Phys. Tech., 67, 371 (2014).

19 C.S. Lim, Mater. Res. Bull., 48, 3805 (2013).

20 J. Sun , J. Xian, X. Zhang, H. Du, J. Rare Earths, 29, 32 (2011).

21 Q. Sun X. Chen, Z. Liu, F. Wang, Z. Jiang, C. Wang, J. Alloys Comp., 509, 5336 (2012).

22 W.C. Oh, J.S. Park, H.S. kim, E.G. Kim, C.S. Lim, J. of Multifunc. Mater. & Photo, 10, 59 (2019).